Integrin αIIbβ3 Reconstituted into Lipid Bilayers Is Nonclustered in Its Activated State but Clusters after Fibrinogen Binding†

Eva-Maria Erb,‡ Kirsten Tangemann,‡ Bernd Bohrmann,§ Beate Müller,‡,|| and Jürgen Engel*,‡

Department of Biophysical Chemistry, Biozentrum of the University of Basel, Klingelbergstrasse 70, CH-4056 Basel, Switzerland, and Pharma Research New Technologies, F. Hoffmann-La Roche, Grenzacherstrasse 124, CH-4002 Basel, Switzerland

Received January 29, 1997; Revised Manuscript Received April 15, 1997⊗

ABSTRACT: Integrin activation, ligand binding, and integrin clustering were analyzed using αIIbβ3 reconstituted into phospholipid vesicles and into supported planar lipid bilayers. Strong and specific binding of fibrinogen and the γ-chain dodecapeptide of fibrinogen to αIIbβ3 indicated that the integrin is in an activated state after membrane reconstitution. Cryoelectron and fluorescence microscopy suggested a nonclustered state of the protein in the vesicle membrane. Supported planar lipid membranes were generated by fusion of vesicles in which approximately equal fractions of integrins were pointing inside-out and outside-in. This distribution led to an immobilization of about 40% of the integrin in supported bilayers due to attachment of the large extracellular domains to the quartz support. Fluorescence recovery after photobleaching indicated a diffusion coefficient of $D = (0.70 \pm 0.06) \times 10^{-8}$ cm^2/s, consistent with a nonclustered state of the mobile integrin. Upon fibrinogen binding, the integrins became immobile, and fluorescence micrographs showed a patchy distribution of fibrinogen−integrin complexes consisting of approximately 250 molecules. In addition to the expected dimer formation by bivalent fibrinogen, additionally induced fibrinogen clustering may account for the large size of the complexes. In contrast, binding of monovalent GRGDS pentapeptide or the γ-chain dodecapeptide of fibrinogen altered neither the mobile fraction nor the association state of αIIbβ3. Our data indicate that integrin αIIbb3 is activated while monodisperse, and became clustered upon fibrinogen binding, leading to an irreversibly bound state.

Integrins comprise a family of heterodimeric membrane-bound receptors which mediate information transfer between cells and their extracellular surrounding (Hynes, 1987) by means of both inside-out and outside-in signaling pathways (Hynes, 1992; Ginsberg et al., 1992). Different mechanisms of activation of these receptors have been proposed, ranging from changes in conformation to assembly of clustered complexes (Diamond & Springer, 1994).

One of the best characterized integrins is αIIbβ3, which is the predominant transmembrane glycoprotein on blood platelets. Binding of fibrinogen to αIIbβ3 leads to platelet aggregation, an important process in the formation of the hemostatic plug. αIIbβ3 binds soluble fibrinogen only after platelet activation by agonists like ATP or thrombin (Marguerie et al., 1979), whereas interaction with immobilized ligand can occur with nonactivated platelets (Savage & Ruggeri, 1991). αIIbβ3 can be reconstituted into phospholipid vesicles (Parise et al., 1985), and into planar lipid bilayers (Müller et al., 1993). *In vitro*, αIIbβ3 was shown to be fully activated, since soluble, monomeric fibrinogen was bound with the same binding characteristics as found for αIIbβ3 on native platelets (Marguerie et al., 1980). The reconstituted integrin binds via a two-step mechanism, comprised of an initial reversible and a subsequent irreversible step (Müller et al., 1993). Analysis of the binding kinetics with surface plasmon resonance and the immobilized integrin confirmed these findings (Huber et al., 1995). The initial reversible complex, the result of a low-affinity interaction, is slowly converted into a more stable and irreversible complex which binds fibrinogen with high affinity. This irreversible binding event was also observed in the physiological interaction between activated platelets and fibrinogen (Marguerie et al., 1980).

In previous studies, binding of antibodies has been shown to change the affinity of integrins for various ligands (Frelinger et al., 1991; Faull et al., 1993). As antibodies also were able to cluster the integrin, the mechanism of activation remained unclear. Experiments with monovalent Fab fragments suggested that clustering was not necessary for activation (O'Toole et al., 1990), although this notion was later challenged by additional experiments indicating that clustering is essential for ligand binding (Sonnenberg et al., 1993). For a number of non-integrin transmembrane receptors like growth factor receptors or the T-cell receptor (Bormann & Engelman, 1992; Heldin, 1995), association and/or autophosphorylation is required for receptor activation and ligand binding. Alternatively, receptor activation may be mediated principally by conformational changes, one of several hypothetical activation mechanisms proposed for integrins (Williams et al., 1994). There is evidence that the intracellular domains of both the α-subunit (O'Toole et al.,

† This work was supported by the Swiss National Science Foundation.

* Correspondence should be addressed to this author at the Department of Biophysical Chemistry, Biozentrum of the University of Basel, Klingelbergstrasse 70, CH-4056 Basel, Switzerland. Phone: 41-61-267 2250. Fax: 41-61-267 2189. Email: Engel@ubaclu.unibas.ch.

‡ Biozentrum of the University of Basel.

§ Pharma Research New Technologies.

|| Present address: Novartis AG, Lichtstrasse 35, CH-4002 Basel, Switzerland.

⊗ Abstract published in *Advance ACS Abstracts,* June 1, 1997.

S0006-2960(97)00218-3 CCC: $14.00

1991; Delwel et al., 1996) and the β-subunit (O'Toole et al., 1994; Hughes et al., 1995) play an important role in integrin activation. However, the structural basis of the activation process remains to be determined.

In the present study, we reconstituted αIIbβ3 in a lipid environment in which the distribution and mobility of the integrin could be monitored directly by electron and fluorescence microscopy. With this system, ligand binding and clustering of the integrins can be analyzed without the interference of cytoplasmic components which might influence the properties of integrins. In addition, the influence of mono- and multivalent ligand binding on the lateral mobility of αIIbβ3 within the supported lipid bilayers could be monitored.

MATERIALS AND METHODS

Materials. Outdated human platelets were obtained from the local blood bank. The integrin αIIbβ3 was purified from detergent extracts of human platelets by anion-exchange and molecular sieve chromatography (Müller et al., 1993). Materials and reagents were purchased from following suppliers: Triton X-100, Sigma (St. Louis, MO); fibrinogen, Chromogenix (Mölndal, Sweden); DMPC,[1] DMPG, and NBD-PE, Avanti Polar Lipids (Alabaster, AL); FITC, TRITC, and the mouse monoclonal antibody against fluorescein, Molecular Probes (Leiden, Netherlands); the synthetic peptide *H*-Gly-Arg-Gly-Asp-Ser-OH, Bachem (Bubendorf, Switzerland); the dodecapeptide of the γ-chain of fibrinogen (γ 400−411) *H*-His-His-Leu-Gly-Gly-Ala-Lys-Gln-Ala-Gly-Asp-Val-OH, Neosystem (Strasbourg, France); Sephadex G-25 M and Sephacryl S-300, Pharmacia LKB Biotechnology (Uppsala, Sweden); Microcons, Amicon (Witten, Germany); Linbro 7X-PF, ICN Flow Biochemicals (Costa Mesa, CA); Bio-Beads SM-2, Bio-Rad (Glattbrugg, Switzerland); quartz slides, Heraeus (Zürich, Switzerland). All other reagents and buffers were obtained from Merck (Darmstadt, Germany), Fluka (Buchs, Switzerland), or Sigma (St. Louis, MO).

Reconstitution of Integrin αIIbβ3 into Lipid Vesicles. A vacuum-dried lipid mixture of DMPG/DMPC (870 nmol, molar ratio 1:1) was solubilized in buffer A (20 mM Tris-HCl, pH 7.4, 50 mM NaCl, and 0.5 mM $CaCl_2$) containing 0.1% Triton X-100. Integrin αIIbβ3 (0.1 mL), 2 mg/mL in buffer A containing 0.1% Triton X-100, was added to 0.9 mL of solubilized lipid (molar ratio lipid:protein = 1000:1). The mixture was shaken for 30 min at 30 °C, followed by 90 min at 37 °C. Triton X-100 was removed by incubating with 50 mg of Bio-Beads for 210 min. After the removal of the beads, a second 50 mg was added for 30 min. Bio-Beads were prewashed with methanol and water as described by Holloway (1973). Nonincorporated αIIbβ3 was separated by ultracentrifugation with a four-step sucrose gradient (2 M, 1.2 M, 0.8 M, and 0.4 M in buffer A) at 4 °C and 275000*g* for 24 h. The visible vesicle-containing fraction within the 0.8 M sucrose step was collected and dialyzed against buffer A. These vesicles were used for electron microscopy.

For FRAP measurements, αIIbβ3 was fluorescently labeled with FITC or TRITC prior to reconstitution into DMPG/DMPC vesicles. The reconstitution protocol described above was used with the following modifications: the integrin−lipid mixture was incubated twice with 25 mg of Bio-Beads SM-2 for 90 and 60 min, respectively. For control FRAP experiments, DMPG/DMPC vesicles (molar ratio 1:1) containing 0.5 mol % NBD-PE were prepared by the extrusion method according to Hope et al. (1985).

Lipid determination was performed with a phosphate assay (Böttcher et al., 1961), and protein concentrations were determined with Folin−Ciacolteau reagent according to Peterson (1977).

Electron Microscopy. For negative staining, vesicle suspensions collected from the sucrose gradient were diluted 5-fold with buffer A, and 10 μL of the solution was placed on a glow-discharged collodium carbon grid. After 3.5 min, 5 μL of 2% sodium phosphotungstate solution, pH 7, was added for 30 s. After removal of the first staining solution, incubation was repeated with 10 μL of the staining solution for 3.5 min.

For cryoelectron microscopy, vesicles were concentrated with a Microcon (Amicon) in an Eppendorf centrifuge to a lipid concentration of 1−2 mg/mL in buffer A according to the suppliers' instructions. Samples of 5 μL were applied to porous carbon films. These films had been prepared by glow-discharge in amylamine vapor (Dubochet et al., 1988) and were supported by rigid 200 mesh copper grids. After removal of excess solution by blotting on filter paper, the grid was rapidly quench-frozen using liquid propane as coolant. The grid was mounted under liquid nitrogen in a side entry specimen holder (Gatan, Model 626 Cryo-Transfer-System), and transferred into a JEOL-1210 electron microscope. Specimens were analyzed and images were recorded at 100 kV accelerating voltage. The analysis of specimens was performed by making use of the minimum dose system (MDS) (Fujiyoshi et al., 1980), designed for recording high-resolution images of radiation-sensitive specimens with minimum electron exposure. The dose rate on each image was measured with a built-in picoamperemeter that measures the current on the fluorescent screen. Images of liposomes were recorded at a magnification of 20000× with an electron irradiation of ∼10 e/Å^2. The objective lens current was adjusted to give an underfocus of approximately 1.5 μm. Digitized micrographs were recorded with a slow-scan CCD camera (Gatan, Model 679). Exposures were made after the stage temperature had reached an equilibrium within the electron microscope, usually after 45 min at ∼−170 °C. Data acquisition with the slow-scan CCD camera and processing of the digitized images were controlled by a Macintosh Quadra 950 computer using the Digital Micrograph program from Gatan. Images were printed on a Thermoprinter Phaser II SD (Tektronix, Wilsonville, USA).

In order to remove gradual variations in overall brightness due to thickness variations of the ice layer, frequency transformations of the images were employed. Brightness variations of the image were assumed to be a low-frequency signal that could be corrected by adequate filtering in the frequency space. This is achieved by excluding the lower

[1] Abbreviations: DMPC, dimyristoylphosphatidycholine; DMPG, dimyristoylphosphatidylglycerol; ECM, extracellular matrix; EM, electron microscopy; FITC, fluorescein 5-isothiocyanate; FRAP, fluorescence recovery after photobleaching; γ 400−411, dodecapeptide of the fibrinogen γ-chain; NBD-PE, *N*-(7-nitro-2,1,3-benzoxadiazol-4-yl)-phosphatidylethanolamine; SDS, sodium dodecyl sulfate; SPB, supported planar bilayer; PAGE, polyacrylamide gel electrophoresis; PE, phosphatidylethanolamine; TIRFM, total internal reflection fluorescence microscopy; Tris, tris(hydroxymethyl)aminomethane; TRITC, tetrametylrhodamine 5(and 6)-isothiocyanate.

spatial frequency components up to 50 nm^{-1} from the higher frequencies and finally retransforming the image.

Average dimensions were determined for 30−50 particles with a semiautomatic image analyzing system coupled to an Apple II computer. The magnification was calibrated using a cross-grating replica (21 600 lines/square; Balzers, Liechtenstein) for the Zeiss EM 9, and catalase crystals for the JEOL 1210.

Fluorescence Labeling of Proteins. Fibrinogen was labeled with fluorescein 5-isothiocyanate (FITC) or tetramethylrhodamine 5(and 6)-isothiocyanate (TRITC) as previously described by Kalb et al. (1990). For FRAP measurements, αIIbβ3 was also labeled with FITC or TRITC prior to reconstitution. In brief, buffer A containing 0.1% Triton X-100 and αIIbβ3 was adjusted to pH 8 by addition of 0.2 M $NaHCO_3$. FITC or TRITC was dissolved in DMSO to a final concentration of 5 mM. A 50-fold molar excess of FITC or TRITC was incubated with the integrin for 30 min in the dark at room temperature. Excess of FITC and TRITC was removed on a Sephadex G-25 M column. The amount of bound FITC or TRITC was determined by measuring the extinction at 493 nm ($\epsilon = 153.8$ cm^2/mg) or 555 nm ($\epsilon = 151.5$ cm^2/mg), respectively. The degree of labeling was between 1 and 2 FITC or TRITC groups per integrin and between 2 and 4 groups per fibrinogen molecule. The fluorescently labeled and nonlabeled fibrinogen showed similar binding affinities to αIIbβ3 as determined in solid phase binding assays (Müller et al., 1993).

Fibrinogen, Peptide, and Antibody Binding to αIIbβ3 Reconstituted into Supported Planar DMPG/DMPC Bilayers. Details of the equipment (Kalb et al., 1990) and the experimental setup (Müller et al., 1993) were described previously. In brief, supported planar bilayers were generated by fusion of DMPG/DMPC vesicles with reconstituted αIIbβ3 onto a quartz slide in the analysis chamber. After being blocked with 1 mg/mL BSA to prevent nonspecific binding to the lipid bilayer, FITC- or TRITC-labeled fibrinogen or monoclonal antibody against fluorescein was injected into the analysis chamber. The time course of the increase or decrease of fluorescence intensity was monitored by total internal reflection fluorescence microscopy (TIRFM), and the equilibrium values were evaluated. All experiments were performed at 33 °C in buffer B (20 mM Tris-HCl, pH 7.4, 150 mM NaCl, and 1 mM $CaCl_2$). The kinetic data were fitted to a two-step binding mechanism (Müller et al., 1993) described by the equation:

$$L + R \underset{k_{-1}}{\overset{k_1}{\rightleftharpoons}} I \xrightarrow{k_2} C$$

Kinetic constants k_1, k_{-1}, and k_2 as fitting parameters were obtained with the program CurveFit (Technosoft, Graz). Previous studies using ultracentrifugation (Rivas et al., 1995) and electron microscopy (Weisel et al., 1992) demonstrated the monovalency of integrin αIIbβ3 for fibrinogen and that fibrinogen has two binding sites for the integrin (Weisel et al., 1992). The affinity of the TRITC-labeled GRGDSPC to integrin αIIbβ3 was previously determined by Müller et al. (1993) to be 2 μM. In an inhibition assay, Pfaff et al. (1994) demonstrated the peptides GRGDSPC and GRGDS to have the same IC_{50} values for αIIbβ3. Binding of the TRITC-labeled dodecapeptide of the fibrinogen γ-chain was performed as described for GRGDSPC.

Fluorescence Recovery after Photobleaching (FRAP). Supported planar bilayers were formed by fusion of vesicles onto the quartz slide according to Brian and McConnell (1984). These membranes were shown to be continuous (Brian & McConnell, 1984), and vesicles adhering to the membrane can be removed by washing with buffer (Kalb & Tamm, 1992). The lateral diffusion coefficients and the mobile fractions of NBD-labeled lipid PE and FITC-labeled αIIbβ3 were determined by FRAP in the epi-illumination mode (Kalb & Tamm, 1992). Unlabeled fibrinogen bound to FITC-labeled αIIbβ3 in supported planar bilayers, and the lateral mobility of the fibrinogen−integrin complex was determined after different times. The diffusion coefficient $D = (4.4 \pm 0.40) \times 10^{-8}$ cm^2/s of the lipid NBD-PE and the complete mobility in both leaflets of the bilayer indicated the intactness of the supported planar membrane and are performed as a control for the used system.

A periodic stripe pattern was produced by focusing a Ronchi ruling of 50 lines per inch in the back-focal image (Smith & McConnell, 1978), resulting in a repeating distance $p = 12.7$ μm. All measurements were performed above the phase transition of the DMPG/DMPC lipid mixture at 33 °C. Individual FRAP curves were fitted by a nonlinear Marquardt routine in combination with a Genetic Algorithm to single exponentials (Tamm & Kalb, 1993) of the type

$$F(t) = F_\infty - (F_\infty - F_0) \exp(-Da^2 t) \qquad (1)$$

The mobile fraction was calculated by

$$m = \left(2 \frac{(F_\infty - F_0)}{F_{pre} - F_0}\right) 100\ \% \qquad (2)$$

where F_∞ is the plateau value of the fluorescence intensity, F_{pre} and F_0 are the fluorescence intensities before and immediately after the bleach pulse, D is the lateral diffusion coefficient, and $a = 2\pi/p$. The factor 2 in eq 2 corrects for the 50% destruction of fluorescent labels in the experimental setup with dark and light stripes of equal width. A fluorescence recovery of 50% represents a mobile fraction of 100%. Typically, six different areas were measured on each sample, and values of three independently prepared samples were averaged. The CurveFit program 1.0 (Technosoft, Graz) was used for data evaluation.

Microphotography. Fluorescence micrographs were taken with a Nicon F601-M camera attached to a FRAP setup on Ilford 400 ASA photographic film in the epi-illumination mode. The film was exposed for 8 s at a low laser illumination intensity and push-processed with an Ilford Microphen developer.

Negatives were scanned with a Leafscan-45 scanner at a magnification of 250 pixels/cm and evaluated with the image analysis program NIH image 1.6. Spots were observed in the range of 0.1−5.08 μm^2. For histograms, submicroscopic particles smaller than 0.19 μm^2 were neglected. All other spots from 0.2 to 5.08 μm^2 were grouped into intervals of 0.2 μm^2.

RESULTS

The Integrin αIIbβ3 Reconstituted into DMPG/DMPC Vesicles Is Not Clustered. DMPG/DMPC vesicles containing reconstituted αIIbβ3 with a molar ratio of protein to lipid of 1:2000 were studied by electron microscopy. Negative

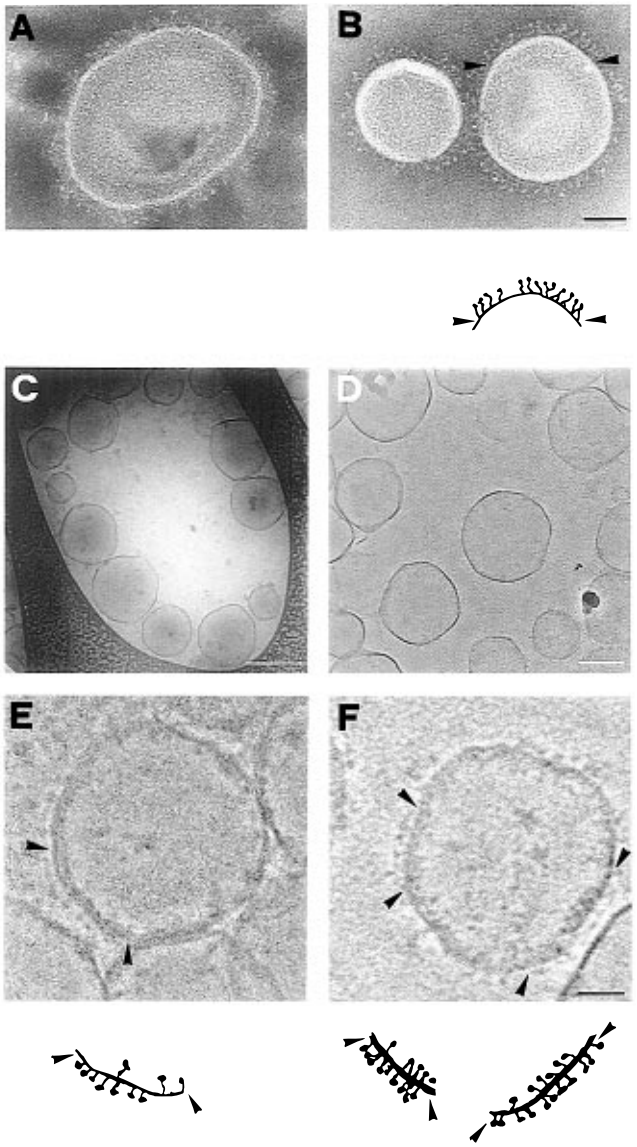

FIGURE 1: Negatively stained and cryoelectron micrographs of DMPG/DMPC vesicles containing integrin αIIbβ3. Negatively stained vesicles with high (A) and with low (B) surface density of integrin αIIbβ3. The bar represents 100 nm. Distribution of vesicles in a vitrified ice layer at the edges of a hole of the carbon film without filter processing of the image (C), and after correction of the thickness variations (D), bars = 200 nm. Cryoelectron micrographs of selected vesicles containing αIIbβ3 (E, F), bar = 50 nm. Schematic drawings represent integrin organization within the membranes of vesicles in panels B, E, and F.

staining of the vesicles yields micrographs with high contrast. Two examples of vesicles with different surface densities are shown in Figure 1A and Figure 1B. At lower surface densities of αIIbβ3 (Figure 1B), well-separated integrin molecules can be clearly distinguished on negatively stained vesicles, indicating a nonclustered monodispersed distribution. The heads of negatively stained αIIbβ3 looked spherical and appeared to have a diameter of about 5.6 nm.

In contrast to negative staining techniques which suffer from the disadvantage that specimens are adsorbed on the grid and became flattened and dehydrated, cryoelectron microscopy (Figure 1C−F) offers the advantage of working with unstained, frozen−hydrated specimens (Dubochet et al., 1988), and the native structure of molecules is preserved. It also provides a tool to observe the interior of the vesicles. The frozen−hydrated liposomes were preferentially localized close to the edges of the holes of the supporting grids (Figure 1C). Unequal brightness originating from variations in the thickness of the layer (Figure 1C) was corrected by image-filtering (Figure 1D). The samples were prevented from cooling below the fluid/crystalline transition temperature of the DMPG/DMPC lipid mixture before injection into the liquid propane to avoid irregularly shaped vesicles with rippled membranes. Visualization of unstained frozen−hydrated proteins requires a distinct underfocus (Dubochet et al., 1988). Optimal resolution of the protein was realized when an underfocus of 1.5 μm was applied. However, the resolution of the bilayer was decreased, in comparison with other focusing conditions which resolved the bilayer into dark inner and outer lines separated by a bright band (result not shown).

Selected vesicles are shown in Figure 1E and Figure 1F. αIIbβ3 molecules can be detected as dark, elongated particles with globular structures connected to the membrane by rods. These structural features are interpreted as the extracellular head and the stalks of integrins. The small cytosolic domains were not visible. The membrane-reconstituted αIIbβ3 was homogeneously distributed and well-separated, indicating a nonclustered, monodispersed state of αIIbβ3. The average diameter of 7.2 ± 1.4 nm in the frozen−hydrated state was slightly larger compared to the value obtained by negative staining, and the heads of the integrins were slightly more elongated in the direction of the membrane plane than in the vertical direction.

In contrast to negatively stained specimens where the stalks appeared to be bent, suggesting a flexible structure, straight rods were seen on cryoelectron micrographs. An about equal number of integrin heads was oriented toward the outside and the inside of the vesicle, indicating a random orientation of the integrin molecules with respect to the lipid membrane. This finding was supported by fluorescence quenching experiments with an antibody against FITC, which reduced the fluorescence intensity by about 50% when added in excess to vesicles containing FITC-labeled αIIbβ3 in suspension (data not shown).

Integrin αIIbβ3 Reconstituted into Supported Planar Bilayers Is Activated. DMPG/DMPC vesicles containing FITC-labeled integrin at a molar ratio of protein to lipid of 1:2000 were fused to quartz slides to generate supported planar bilayers. Fluorescence micrographs taken from these bilayers showed a homogeneously distributed fluorescence intensity with only minor granularity (see below). This indicates that the reconstituted αIIbβ3 in supported planar bilayers appears to be incorporated as was previously demonstrated for lipid vesicles (Müller et al., 1993). After vesicle fusion, the time course of binding of 90 nM TRITC-labeled fibrinogen to reconstituted αIIbβ3 in supported planar bilayers was monitored by TIRFM (Figure 2) as previously described (Müller et al., 1993). The kinetics were fitted to a two-step binding mechanism, and the same kinetic parameters were found for the unlabeled, the TRITC-labeled (data not shown), and the FITC-labeled integrin: $k_1 = 1.97 \times 10^4$ M^{-1} s^{-1}, $k_{-1} = 8.08 \times 10^{-4}$ s^{-1}, $k_2 = 3.5 \times 10^{-4}$ s^{-1}, and $K_D = k_{-1}/k_1 = 41$ nM. Similarly, in solid phase binding assays, the same fibrinogen binding activity was found for labeled and unlabeled αIIbβ3 (results not shown). These data indicate that fluorescence labeling and membrane reconstitution did not alter the ligand binding properties of αIIbβ3.

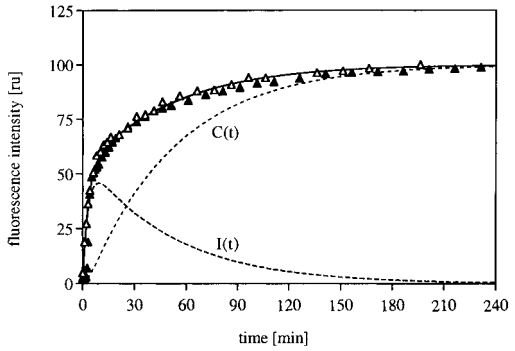

FIGURE 2: Kinetics of association of TRITC-labeled fibrinogen with nonlabeled αIIbβ3 (▲) and with FITC-labeled αIIbβ3 (△) reconstituted into supported planar bilayers by TIRFM. The time course of the binding of 90 nM TRITC-labeled fibrinogen to the integrin was followed by measuring the increase of fluorescence intensity. In experiments using FITC-labeled αIIbβ3, the fluorescence intensity was corrected by the value obtained for the background signal of fluorescently labeled integrin. A single representative experiment out of five independent experiments is shown. The experimental data were fitted to the biphasic kinetics by a two-step mechanism where $I(t)$ represents the time course of formation of the reversible complex and $C(t)$ of the final irreversible complex.

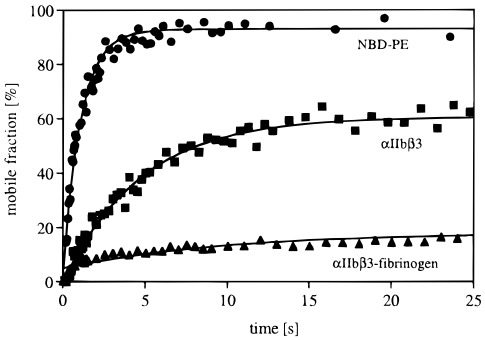

FIGURE 3: Determination of the lateral diffusion coefficients of FITC-labeled αIIbβ3, αIIbβ3−fibrinogen complexes, and NBD-labeled PE incorporated into DMPG/DMPC bilayers. The time courses of fluorescence recovery after photobleaching in supported planar DMPG/DMPC bilayers containing 0.5 mol % NBD-labeled PE (●), FITC-labeled αIIbβ3 (■), and FITC-labeled integrin αIIbβ3 incubated with 90 nM unlabeled fibrinogen for 180 min (▲) were fitted to single exponential curves. All values are determined at 33 °C.

Integrin αIIbβ3 Reconstituted into Supported Planar Bilayers Is Mobile. Fluorescence recovery after photobleaching (FRAP) experiments with NBD-labeled PE and FITC-labeled αIIbβ3 incorporated into supported planar bilayers of DMPG/DMPC were performed to determine the lateral mobility of PE, αIIbβ3, and αIIbβ3 in the presence of fibrinogen. The FRAP curves shown in Figure 3 were determined at 33 °C and were fitted to single exponentials (continuous curves). By fusion of DMPG/DMPC vesicles containing 0.5 mol % NBD-PE to quartz slides, supported planar bilayers labeled with homogeneously distributed NBD-PE were generated. From FRAP experiments, a diffusion coefficient $D = (4.4 \pm 0.40) \times 10^{-8}$ cm^2/s with a mobile fraction of $m = (93 \pm 7)\%$ was calculated. These values are in close agreement with earlier data obtained by Kalb et al. (1992) and Tamm (1988) and clearly indicate that most of the fluorescently labeled lipid in both leaflets of the supported bilayer is mobile. Measurements of the FITC-labeled αIIbβ3 reconstituted into the DMPG/DMPC bilayer yielded a diffusion coefficient of $D = (0.70 \pm 0.06) \times 10^{-8}$ cm^2/s and a mobile fraction $m = (57 \pm 9)\%$.

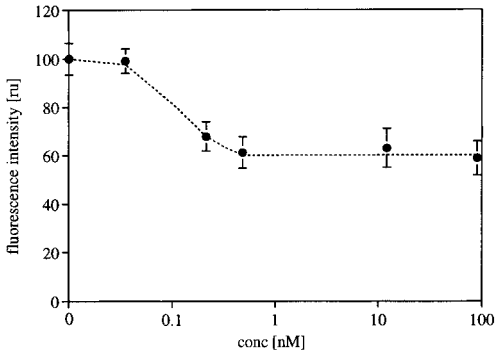

FIGURE 4: Determination of the orientation of integrins in a supported lipid bilayer. The accessibility of FITC molecules covalently bound to αIIbβ3 was assayed with an excess of a quenching monoclonal antibody against fluorescein. The decrease in fluorescence intensity was plotted against the concentration of quenching antibody. Shown are the mean values and standard deviations of five individual experiments.

The accessibility of FITC molecules covalently bound to αIIbβ3 was evaluated with an anti-fluorescein quenching antibody (Figure 4). About 90% of the lysines and arginine residues, which represent potential FITC-reactive sites on αIIbβ3, are located on the extracellular part of the molecule (Poncz et al., 1987; Lanza et al., 1990). An excess of anti-fluorescein monoclonal antibody reduced the fluorescence intensity by (40 ± 8)%, indicating that at least 40% of the integrin molecules were oriented with their heads toward the solution and competent to bind ligands. These data indicate that the distribution of reconstituted αIIbβ3, with equal numbers of integrin molecules facing into or out of the vesicle, is conserved after fusion of the vesicles onto quartz slides.

Fibrinogen Binding to Membrane-Reconstituted αIIbβ3 Mediates Clustering and Immobilization of the Receptor−Ligand Complexes. 90 nM unlabeled fibrinogen was bound to FITC-labeled αIIbβ3, and the diffusion coefficient and the fraction of mobile integrin−ligand complex were evaluated after different periods of interaction (Figures 3, 5A). The mobile fraction decreased from $F = (57 \pm 9)\%$ to (18 ± 5)% after 300 min, which corresponds to a reduction of 70% of the initial mobile fraction (Figure 5A). The lateral diffusion coefficient of the 30% mobile fraction of $D = (0.58 \pm 0.06) \times 10^{-8}$ cm^2/s was only slightly lower than that of the ligand-free integrin. It should be noted that about 30% of the integrins are expected to be liganded-free at a fibrinogen concentration of 90 nM. A fibrinogen concentration of 30 nM, corresponding to a receptor saturation of 60%, resulted in a reduction of 40% of the initial mobile fraction (Figure 5A). The time course of immobilization is in agreement with the formation of the irreversible complex, the second step in the binding of fibrinogen to αIIbβ3 (Figure 5B; Müller et al., 1993). The small sigmoidal initial phase is shown in both time courses although in the immobilization experiment the error limits in this range are rather large. In contrast to fibrinogen, the binding of 5 μM GRGDS pentapeptide or 2.3 μM of the dodecapeptide of the fibrinogen γ-chain, γ 400−411, which yield the same degree of saturation of αIIbβ3 as 90 nM fibrinogen, did not show any effect on the lateral diffusion coefficient (Table 1) and the mobile fraction of αIIbβ3 (Figure 5A).

In parallel with the determination of diffusion coefficients and mobile fractions, the homogeneity of the distribution of

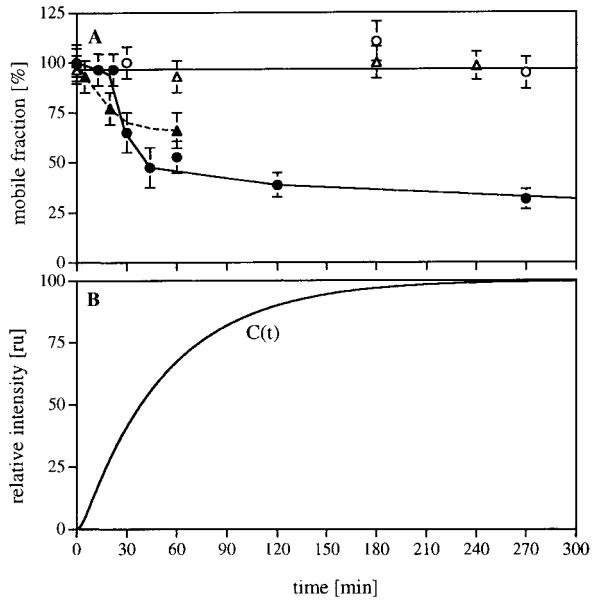

FIGURE 5: (A) Determination of the mobile fraction of αIIbβ3 and complexes of αIIbβ3 with fibrinogen, GRGDS pentapeptide, or the γ-chain dodecapeptide of fibrinogen, γ 400−411. 90 nM unlabeled fibrinogen (●), 30 nM unlabeled fibrinogen (▲), 5 μM GRGDS (○), or 2.3 μM γ 400−411 (△) was added to FITC-labeled, membrane-reconstituted αIIbβ3 and the mobile fraction evaluated at different time points of interaction. Mobile fractions are expressed as percent of the mobility before addition of the ligands. (B) The decrease in mobile fraction after fibrinogen binding correlates with the formation of the irreversible complex $C(t)$ of the receptor−ligand binding, calculated according to the two-step binding mechanism of fibrinogen binding to integrin.

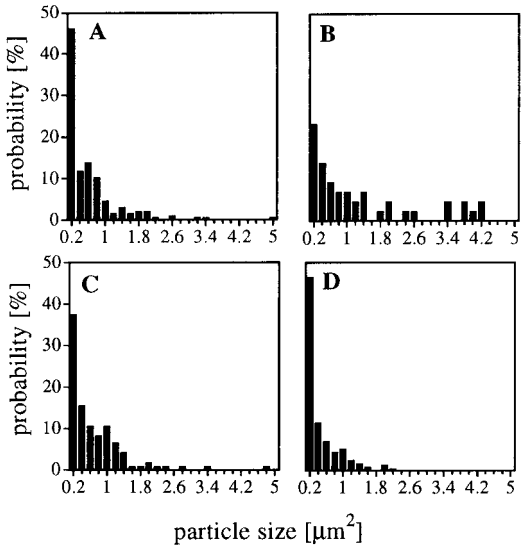

FIGURE 6: Histograms of selected fluorescence micrographs showing the size distribution of fluorescent particles. Spots above the size of submicroscopic particles (0.19 μm^2) were grouped in intervals of 0.2 μm^2. (A) FITC-labeled αIIbβ3 alone, (B) incubated with 90 nM nonlabeled fibrinogen, (C) 5 μM GRGDS, and (D) 2.3 μM γ 400−411.

FITC-labeled αIIbβ3 within the supported planar bilayers was analyzed. Histograms showing the size distribution of fluorescent particles demonstrate clearly that in the presence of 90 nM fibrinogen (Figure 6B) the particle size is shifted to larger size groups (1.8 −4.2 μm^2) and the number of monodispersed particles is reduced, indicating the formation of clusters. Their areas of up to 4.2 μm^2 correspond to clusters of up to 250 fibrinogen molecules. In the absence of ligand (Figure 6A), as well as in the presence of 5 μM GRGDS pentapeptide (Figure 6C) or 2.3 μM γ 400−411 (Figure 6D), the fluorescent particles were mainly of smaller diameter (<1 μm^2), indicating contributions of submicroscopic monomers (0.2 μm^2) and small aggregates. Thus, clustering of αIIbβ3 is specifically mediated by fibrinogen binding. The influence of ligand binding on the diffusion coefficient, the mobile fraction, and clustering is summarized in Table 1.

DISCUSSION

In the present study, it was investigated whether activated αIIbβ3 is clustered in the absence or presence of ligands when incorporated into lipid vesicles and supported planar bilayers. We used cryoelectron microscopy to determine the distribution of integrin in phospholipid vesicles and found them well separated and equally distributed. If we estimate the cross-sectional area of the transmembrane domain of αIIbβ3 to be 1.3 nm^2 (Gonzalez-Rodriguez et al., 1994), and the diameter of the integrin head to be 5.6−7.2 nm, the minimum distance between two integrin heads can be calculated to be 18−20 nm. By electron microscopy of negatively stained vesicles, distances of 25 nm without any contacts between the extracellular head regions were found, suggesting monodispersed distribution of the αIIbβ3 within the membrane. The globular heads and long stalks protruding from the membrane are likely to represent the extracellular domains of the integrins. The cytosolic domains are too small to be resolved. About equal numbers of extracellular heads were pointing out of the vesicles as were into the interior, suggesting a random orientation of the integrins within the vesicle membrane. This nonselective orientation was supported by quenching experiments using an antibody against FITC, in which about 50% of the FITC molecules bound to αIIbβ3 were shown to be accessible.

The fluorescence microsopic techniques, TIRFM and FRAP, were employed to determine ligand binding properties and to compare the diffusion behavior of the integrin alone and complexed with different ligands. FITC labeling of αIIbβ3 did not alter the ligand binding properties of the integrin. A two-step binding mechanism with an initial reversible and a subsequent irreversible step was previously observed for membrane-reconstituted αIIbβ3 (Müller et al., 1993), similar to studies of αIIbβ3 in ATP-activated platelets (Marguerie & Plow, 1981). Fibrinogen binds to reconstituted αIIbβ3 with the same affinity as to activated integrin in platelets (Marguerie et al., 1979). The ligand-free integrin was found to be monodisperse as indicated by the small diameter of the fluorescent particles. In previous microscopic studies (Loftus & Albrecht, 1984; Isenberg et al., 1987), the activated integrin was shown to be monodisperse on activated and spread platelets. These findings indicate that activated integrin is nonclustered and that clustering is not required for activation.

A monodisperse distribution of activated αIIbβ3 was also indicated by measurements of the mobility with the FRAP technique. Fifty percent of the integrin population was found to be mobile, and the immobility of the remaining population is consistent with integrins inserted in the opposite direction, allowing attachment of their large extracellular domains to the quartz support of the membranes. Concerning the mobile fraction, the small size of the cytoplasmic domains prevented the integrin from sticking to the support. The lateral

Table 1: Summary of Kinetic Constants, Reduction of Mobile Fractions, Effect on Clustering and Diffusion Coefficients of Ligands to αIIbβ3

ligand	fast reversible step, K_D (nM)	slow irreversible step	reduction of mobile fraction (%)	clustering	diffusion coefficient ($10^{-8} \times cm^2/s$)
no ligand				no	0.70 ± 0.06
fibrinogen	40	yes	70	yes	0.58 ± 0.06
GRGDS[a]	2000	no	0	no	0.75 ± 0.05
dodecapeptide γ-chain	1000	no	0	no	0.66 ± 0.10

[a] The binding affinity was determined by Müller et al. (1993) and Pfaff et al. (1994).

diffusion coefficient of the integrin was found to be only 6 times smaller than that of the lipid. The value of 0.70×10^{-8} cm^2/s corresponds well with values found for other monodisperse membrane-spanning proteins at comparable surface concentrations (Vaz et al., 1984). Lateral diffusion coefficients of integrins have also been measured in various cell types (Duband et al., 1988; Schootemeijer et al., 1993; Schmidt et al., 1995). They are 17−35 times smaller than the value obtained for the reconstituted αIIbβ3. Similar differences between mobilities in native cell membranes and artificial membranes were found for other receptors. For example, the transmembrane protein pgp-1, a member of the CD 44 protein family, diffuses 100 times faster in artificial membranes (Zhang et al., 1993) than in its native environment. The reduced diffusion coefficients in cell membranes may be due to interactions with relatively immobile structures such as the cytoskeleton (Clark & Brugge, 1995), by steric hindrance due to membrane-associated molecules (Brown et al., 1990), or by highly viscous microdomains of the cell membrane that retard lateral diffusion (Sheets et al., 1995).

Binding of 90 nM fibrinogen to αIIbβ3 reduces the mobility by about 70%. A fibrinogen concentration of 30 nM results in an decreased mobile fraction of 60%. The remaining mobile fraction corresponds to the fraction of ligand-free integrin which is present under the experimental conditions, 30% at a fibrinogen concentration of 90 nM and 60% at a fibrinogen concentration of 30 nM. The ligand-free state of the mobile fraction is also demonstrated by the diffusion coefficient of the mobile population, identical to that of the free integrin. The complete immobilization of the αIIbβ3−fibrinogen complex cannot be due to cross-linking of the integrins by the bivalent fibrinogen since in model studies with other dimerizing agents only reductions of the diffusion coefficient by a factor of 2 were observed (Tamm, 1988; Zhang et al., 1991). Clustering may be induced by lateral association of fibrinogen-liganded integrins as well as by the interaction between an integrin-bound fibrinogen and a second fibrinogen molecule. In solution, fibrinogen was monomeric as shown by ultracentrifugation, and there was no indication of fibrinogen aggregation on plain lipid bilayers. The large size of the clusters shown in the histogram is consistent with both interactions. The association of ligands and/or receptors may be coupled to conformational changes of the integrin leading to the exposure of ligand-induced binding sites (LIBS; Frelinger et al., 1991; Loftus et al., 1987), or of fibrinogen leading to the exposure of receptor-induced binding sites (RIBS; Ugarova et al., 1993; Zamarron et al., 1991). Interestingly, clustering correlates with the occurrence of a second binding step. The essential irreversibility of the binding event following this step may be a result of lateral association of fibrinogen−integrin complexes leading to cluster formation with a very slow release of fibrinogen from clusters. No clustering was induced by binding of the small ligands GRGDS and the γ-chain dodecapeptide, which bind reversibly in a one-step mechanism to αIIbβ3. On the other hand, Isenberg et al. (1987) observed by immunomicroscopy clustering of αIIbβ3 by GRGDS pentapeptide and the γ-chain decapeptide, which do not exhibit a second slow binding step. These results were obtained on native platelets and thus in the presence of other potential reaction partners. Further studies analyzing the interactions between the cytoplasmic domains of the integrins and their ligands will be necessary to determine the molecular mechanism of integrin clustering.

ACKNOWLEDGMENT

We thank Robert Häring for image analysis, Dr. Heike Hall and Dr. Markus Dürrenberger for helpful discussion, and Dr. Jay Groppe and Dr. Heike Hall for critically reading the manuscript.

REFERENCES

Bormann, B. J., & Engelman, D. M. (1992) *Annu. Rev. Biophys. Biomol. Struct. 21*, 223−242.
Böttcher, C. J. F., Van Gent, C. M., & Fries, C. (1961) *Anal. Chim. Acta 24*, 203−204.
Brian, A. A., & McConnell, H. M. (1984) *Proc. Natl. Acad. Sci. U.S.A. 81*, 6159−6163.
Brown, E., Hooper, L., Ho, T., & Gresham, H. (1990) *J. Cell Biol. 111*, 2785−2794.
Clark, E. A., & Brugge, J. S. (1995) *Science 268*, 233−239.
Delwel, G. O., Hogervorst, F., & Sonnenberg, A. (1996) *J. Biol. Chem. 271*, 7293−7296.
Diamond, M. S., & Springer, T. A. (1994) *Curr. Biol. 4*, 506−517.
Duband, J.-L., Nuckolls, G. H., Ishihara, A., Hasegawa, T., Yamada, K. M., Thiery, J. P., & Jacobson, K. (1988) *J. Cell Biol. 107*, 1385−1396.
Dubochet, J., Adrian, M., Chang, J.-J., Homo, J.-C., Lepault, J., McDowall, A. W., & Schultz, P. (1988) *Q. Rev. Biophys. 21*, 129−228.
Faull, R. J., Kovach, N. L., Harlan, J. M., & Ginsberg, M. H. (1993) *J. Cell Biol. 121*, 155−162.
Frelinger, A. L., III, Du, X. P., Plow, E. F., & Ginsberg, M. H. (1991) *J. Biol. Chem. 266*, 17106−17111.
Fujiyoshi, Y., Kobayashi, T., Uyeda, N., IIshida, Y., & Harada, Y. (1980) *Ultramicroscopy 5*, 459−468.
Ginsberg, M. H., Du, X., & Plow, E. F. (1992) *Curr. Biol. 4*, 766−771.
Gonzalez-Rodriguez, J., Acuna, A. U., Alvarez, M. V., & Jovin, T. M. (1994) *Biochemistry 33*, 266−274.
Heldin, C.-H. (1995) *Cell 80*, 213−223.
Holloway, P. W. (1973) *Anal. Biochem. 53*, 304−308.
Hope, M. J., Bally, M. B., Webb, G., & Cullis, P. R. (1985) *Biochim. Biophys. Acta 812*, 55−65.
Huber, W., Hurst, J., Schlatter, D., Barner, R., Hübscher, J., Kouns, W. C., & Steiner, B. (1995) *Eur. J. Biol. Chem. 227*, 647−656.
Hughes, P. E., O'Toole, T. E., Ylänne, J., Shattil, S. J., & Ginsberg, M. H. (1995) *J. Biol. Chem. 270*, 12411−12417.
Hynes, R. O. (1987) *Cell 48*, 549−554.
Hynes, R. O. (1992) *Cell 69*, 11−25.
Isenberg, W. M., McEver, R. P., Phillips, D. R., Shuman, M. A., & Bainton, D. F. (1987) *J. Cell Biol. 104*, 1655−1663.

Kalb, E., & Tamm, L. K. (1992) *Thin Solid Films 210/211*, 763−765.
Kalb, E., Engel, J., & Tamm, L. K. (1990) *Biochemistry 29*, 1607−1613.
Kalb, E., Frey, S., & Tamm, L. K. (1992) *Biochim. Biophys. Acta 1103*, 307−316.
Lanza, F., Kieffer, N., Phillips, D. R., & Fitzgerald, L. A. (1990) *J. Biol. Chem. 265*, 18098−18193.
Loftus, J. C., & Albrecht, R. M. (1984) *J. Cell Biol. 99*, 822−829.
Loftus, J. C., Plow, E. F., Frelinger, A. L., III, D'Souza, S. E., Dixon, D., Lacy, J., Sorge, J., & Ginsberg, M. H. (1987) *Proc. Natl. Acad. Sci. U.S.A. 84*, 7114−7118.
Marguerie, G. A., & Plow, E. F. (1981) *Biochemistry 20*, 1074−1080.
Marguerie, G. A., Plow, E. F., & Edgington, T. S. (1979) *J. Biol. Chem. 254*, 5357−5363.
Marguerie, G. A., Edgington, T. S., & Plow, E. F. (1980) *J. Biol. Chem. 255*, 154−161.
Müller, B., Zerwes, H. G., Tangemann, K., Peters, J., & Engel, J. (1993) *J. Biol. Chem. 268*, 6800−6808.
O'Toole, T. E., Loftus, J. C., Du, X., Glass, A. A., Ruggeri, Z. M., Shattil, S. J., Plow, E. F., & Ginsberg, M. H. (1990) *Cell Regul. 1*, 883−893.
O'Toole, T. E., Mandelman, D., Forsyth, J., Shattil, S. J., Plow, E. F., & Ginsberg, M. H. (1991) *Science 254*, 845−847.
O'Toole, T. E., Katagiri, Y., Faull, R. J., Peter, K., Tamura, R., Quaranta, V., Loftus, J. C., Shattil, S. J., & Ginsberg, M. H. (1994) *J. Cell Biol. 124*, 1047−1059.
Parise, L. V., & Phillips, D. R. (1985) *J. Biol. Chem. 260*, 1750−1756.
Peterson, G. L. (1977) *Anal. Biochem. 83*, 346−356.
Pfaff, M., Tangemann, K., Müller, B., Gurrath, M., Müller, G., Kessler, H., Timpl, R., & Engel, J. (1994) *J. Biol. Chem. 269*, 20233−20238.
Poncz, M., Eisman, R., Heidenreich, R., Silver, S. M., Vilaire, G., Surrey, S., Schwartz, E., & Benett, J. S. (1987) *J. Biol. Chem. 262*, 8476−8482.
Savage, B., & Ruggeri, Z. M. (1991) *J. Biol. Chem. 266*, 11227−11233.
Schmidt, C. E., Horwitz, A. F., Lauffenburger, D. A., & Sheetz, M. P. (1995) *J. Cell Biol. 123*, 977−991.
Schootemeijer, A., Gorter, G., Tertoolen, L. G., van Willigen, G., de-Laat, S. W., & Akkerman, J. W. (1993) *Thromb. Haemostasis 69*, 784.
Sheets, E. D., Simson, R., & Jacobson, K. (1995) *Curr. Biol. 7*, 707−714.
Smith, J. W., & McConnell, H. M. (1978) *Proc. Natl. Acad. Sci. U.S.A. 75*, 2759−2776.
Sonnenberg, A., de Melker, A. A., Martinez de Velasco, A. M., Janssen, H., Calafat, J., & Niessen, C. M. (1993) *J. Cell Sci. 106*, 1083−1102.
Tamm, L. K. (1988) *Biochemistry 27*, 1450−1457.
Tamm, L. K., & Kalb, E. (1993) *Chem. Anal. (N.Y.) 77*, 253−305.
Ugarova, T. P., Budzynski, A. Z., Shattil, S. J., Ruggeri, Z. M., Ginsberg, M. H., & Plow, E. F. (1993) *J. Biol. Chem. 268*, 21080−21087.
Vaz, W. L. C., Goodsaid-Zalduondo, F., & Jacobson, K. (1984) *FEBS Lett. 174*, 199−207.
Weisel, J. W., Najaswami, C., Vilaire, G., & Bennett, J. S. (1992) *J. Biol. Chem. 267*, 16637−16643.
Williams, M. J., Hughes, P. E., O'Toole, T. E., & Ginsberg, M. H. (1994) *Trends Cell Biol. 4*, 109−112.
Zamarron, C., Ginsberg, M. H., & Plow, E. F. (1991) *J. Biol. Chem. 266*, 16193−16199.
Zhang, F., Crise, B., Su, B., Hou, Y., Rose, J. K., Bothwell, A., & Jacobson, K. (1991) *J. Cell Biol. 115*, 75−84.
Zhang, F., Lee, G. M., & Jacobson, K. (1993) *Bioessays 15*, 579−88.

BI9702187